Ring Compression Tests of Insituform IMain Liner

Prepared by

Cornell University NEESR Group

September 2, 2011

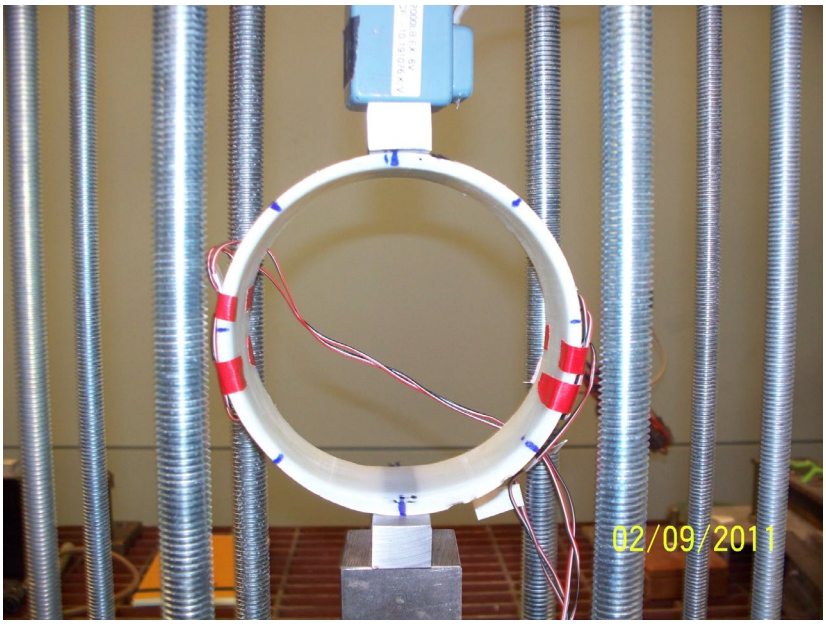

TABLE OF CONTENTS

LIST OF PHOTOS

LIST OF TABLES

LIST OF FIGURES

Ring Compression Testing

1. Introduction

Ring compression tests were performed on 2-in.-wide circular sections of the Insituform IMain pipe liners. The composition of the rings was IMain epoxy resin with IMain hardener. The ring sections were cut from longer tubular sections of the liner that had been cast in a cylindrical cardboard mold, most likely a Sonotube, and then removed from the cardboard mold. InsituForm Technologies, Inc. prepared the tubular sections and shipped them to Cornell. The purpose of the testing was to evaluate the transverse bending stiffness of the composite liners and to evaluate the variations in liner geometries and the effect of those variations on stiffness characteristics. Eight rings were tested. The specimen numbering system and test descriptions are given in Table 1.

The rings were placed in a servo-hydraulic loading system and loaded vertically at the top and bottom. Load was measured with a load cell attached to the hydraulic actuator. Photo 1 shows the experimental setup for the ring tests. The top and bottom of the ring were fitted with 1-in.-wide metal loading fixtures that were machined to fit the nominal curvature of the rings. This resulted in roughly a 5º contact angle over the top and bottom of the rings, which was sufficiently large to avoid localized damage or failure, but small enough to consider the top and bottom contacts as point loadings, particularly when considering springline responses. Vertical displacements were measured with the internal LVDT within the actuator. All of the specimens were loaded initially with the thickest part of the ring at the 180º degree position and 0º at the top. The specimens were loaded in displacement control, with incremental loading and unloading cycles.

2. Specimen 1st 1 Ring Test

Wall thickness measurements were made at 15º intervals clockwise (as viewed from Photo 1) around the circumference of the ring. Figure 1 shows the variation in wall thickness for specimen 1st 1. In Figure 1 the 0º location was taken as the top of the ring when loaded in compression. Note that the liner is stitched together at two locations, which are not 180º apart. The average wall thickness was t_W = 0.257 in. with a standard deviation of 0.047 in. If the wall thickness measurements within ± 15º of the threads are not included in the averaging, the average wall thickness drops to 0.248 in., which is only 3% less than when all measurements are used. It is important to note that the average wall thickness for the 0º to 180º half of the ring is 0.273 in. whereas the average thickness of the 180º to 360º half is 0.243 in. On average, the 0º to 180º half of the ring is roughly 12% thicker than the 180º to 360º half.

The ring was placed in a servo-hydraulic loading system and loaded vertically at the top and bottom (see Photo 1). Four cycles of load were applied with peak forces of roughly 15, 20 and 30 lb. Figure 2 shows the force and displacement versus time for the four load cycles. Note that there is some residual displacement of the ring following the first load cycle.

Figures 3a to 3c shows the vertical force- displacement relationships measured during the four load cycles. The force-displacement relationships are nearly identical for the four cycles as indicated by the slope of the lines in Figure 3.

Strain gage rosette pairs mounted at the springline positions to measure strains in the hoop (circumferential) and axial (longitudinal) directions. The axial (longitudinal) direction is parallel to the initial long axis of the liner sections from which the rings were cut. Gages Axial 0 and Hoop 1 were a pair, and Axial 2 and Hoop 3 were the other pair. Figure 4 shows the force-strain measurements for the four load cycles. The force-strains are nearly identical for the four cycles, as

indicated by the slopes of the lines given in Table 2. Table 2 also gives the average slopes along with the standard deviation and coefficient of variation (COV = standard deviation / mean).

The specimen was later tested at various orientations. Tests were performed at the alignment as before, with the 0º location at the top and the 180º location at the bottom. The ring was then rotated in 45º increments and tested. The initial 90º and 270º springline locations were not tested because these were the locations of the strain gages. While strains were measured at all ring orientations, only those in which the ring was at 0º and 180º at the top can be readily interpreted. For these tests, two load cycles were applied at each ring orientation.

Figures 5a to 5g show the force-displacement results for these ring tests. Table 3 gives the slopes and ring stiffnesses of the force-displacement tests for the various angles. The differences in stiffnesses clearly are affected by the changes in wall thickness of the ring. Figure 6 shows the variation in stiffness versus circumferential angle. The stiffnesses are roughly symmetric about the 180º position, as would be expected. The variations are due to the variations in wall thickness. The repeat test at 360º shows a stiffness roughly 4% lower than the initial test at 0º, which was the same nominal ring orientation. This difference is small, and within the acceptable experimental variation.

Figures 7a to 7g show the force-strain measurements made when the ring was positioned at various angles. Table 4 lists the position of the gage pairs relative to the top load point of the ring. The Hoop 3 gage of the repeat 360º (0º) (Fig. 7g) measurement appears faulty for the repeat cycle of loading. The slopes of the force-strain data from the 0º angle are given in Table 5, which is identified as the second testing event in which the ring was orientated at various angles. These gage responses are in good agreement with the first testing event of ring 1st 1 (see Table 2) when multiple cycles were applied.

3. Ring Tests 1st 2 through 3S

The seven other rings did not incorporate strain gages, and were tested with the thickest part of the ring in the 180º position. Specimen 1st 2 was taken from a liner section adjacent to specimen 1st 1. The pairs 1N and 1S, 2N and 2S, and 3N and 3S were taken from opposite ends of the roughly 8-ft-long sections. Figure 8 shows the wall thicknesses and diameter of all rings. In the figures the wall thickness for the 0º position was also used as the thickness at the 360º position. Similarly, the diameter at the 0º position was also used as the diameter at the 180º position. Table 6 gives the measured values. The global average wall thickness was t_W = 0.266 in. with a standard deviation of 0.038 in. The global average diameter was D = 6.000 in. with a standard deviation of 0.024 in, Note that D = 6.0 in was the nominal inside diameter of the Sonotubes used to mold the specimens.

Figure 9a shows the force-displacement results for Specimen 1st 2. There is slight nonlinearity beginning at an applied force of roughly 60 lb. At the peak force of approximately 100 lb there was a slight crack in the outer epoxy, as indicated by the reduction in force.

Figures 9b and 9c show the force-displacement results for Specimens 1N and 1S. These specimens, taken from opposite ends of a liner section, showed very similar results. The same is true for Specimens 2N and 2S, shown in Figures 9d and 9e.

Figures 9f and 9g show the force-displacement test results from Specimens 3N and 3S. Specimen 3N data are similar to 1N, 1S, 2N and 2S. Specimen 3N developed a delamination at the 270º springline at a load of roughly 50 lb. Photo 2 shows this delamination. Photo 3 shows an apparent defect in the liner at the 270º springline. This appears to be a burn of some type. Photo 4 shows this defect in the space between the lining materials.

4. Tests to Failure

Specimens 1N, 1S, and 1st 2 were loaded to failure. In these tests, the rings were placed in the loading system and deformed to the practical limit of the testing system. Figure 10 shows the force-displacement results from these three tests. All test showed nearly linear response up to a force of 80 lb. At a force of roughly 120 lb there was audible cracking of the outer epoxy and a noticeable drop in the force, followed by an increase in the force and additional cracking.

Photos 5, 6, and 7 show specimen 1S at various levels of deformation. In all cases the outer springline was the critical location. There were no observed cracks or tears on the inner springlines.

5. Data Interpretation

The ring tests described in this report were performed on sections taken from the liner that had been cast in nominal 6-in.-inner diameter Sonotubes. Thus, they do not necessarily reflect the characteristics of the liner cast in the DI test pipes. However, the tests do capture general characteristics of the liner material. The liner thicknesses and diameters are variable. The global average wall thickness was t_W = 0.266 in. with a standard deviation of 0.038 in. The global average diameter was D = 6.000 in. with a standard deviation of 0.024 in.

A main interest in the ring tests was to estimate the flexural modulus of the composite lining. The expression for the vertical displacement of the ring (Young, 1989) is given by:

$$\delta_V = 0.1488 \frac{Fr^3}{EI} \qquad (1)$$

in which F is the force, r is the average radius, E is Young's modulus, and I is the transverse moment of inertia. For the ring $I = t_W^3/12$ in which t_W is the wall thickness.

Equation 1 can be rearranged to:

$$E = 0.1488 \frac{Fr^3}{\delta_V \left(t_W^3 / 12 \right)} = 0.1488 \frac{F}{\delta_V} \frac{r^3}{\left(t_W^3 / 12 \right)} \quad (2)$$

For simplicity, use the global average wall thickness of t_w = 0.266 in. and global average diameter of D = 6.00 in. Taking the slopes of the force-displacement test results, $\Delta F/\Delta\delta_V$, as F/δ_v in Equation 2, the average radius of r = 3.00 in. and the average wall thickness of t_W = 0.266 in. Equation 2 can be used to estimate a Young's modulus, E, in flexure. Tables 7 and 8 give the ring stiffness and computed moduli for the tests, respectively. The moduli range from roughly 420 to 690 ksi, with an average value of 540 ksi. The values could be adjusted based on the local wall thickness at the springline location. However, the ring tests include some averaging of the wall thicknesses around the ring since the entire specimen in involved in the compression and distribution of stresses throughout. The average value of 540 ksi is higher that the flexural modulus of 451 ksi reported by Insituform (see K. Costa's email 11/16/10).

6. Additional Measurements

A ring section was cut from a liner section adjacent to the location from which Specimen 1st 1 was taken. Wall thickness measurements were taken and they were nearly identical to those shown in Figure 1 for specimen 1st 1. Figure 11 shows polar plots of the cross-sectional geometries of Specimen 1st 1 and the Untested specimen. The locations of the threads are shown on the figure and the thick areas near the 180º locations are visible.

The gage pair strains for the first four cycles of loading for Specimen 1st 1 are shown in Figure 12. The figure shows axial versus hoop strains for gage pairs Ax. 0 and Hoop 1, which are at the 90º position and gage pairs Ax. 2 and Hoop 3, which are at the 270º position. The slopes of these data

are given in Table 9. The Ax. 0 and Hoop 1 pair have similar slopes for cycles 1 and 3, but the slopes are different for cycles 2 and 4. The cause of this variation for gage pairs Ax. 0 and Hoop 1 between cycles is not known. The slopes of gage pairs Ax. 2 and Hoop 3 are nearly identical for each of the four cycles. The data shown in Table 2 and Figure 4 for Specimen 1st 1 gave the slopes of the force – strain data, which were shown in Figure 4.

The slopes of the force-strain data in Table 2 (based on Figure 4) are given in terms of $\Delta F/\Delta\mu\varepsilon$ (lb/με). These data can be used to compare the data given in Table 9 and Figure12 by:

$$\frac{(\Delta F/\Delta\mu\varepsilon)_{Hoop}}{(\Delta F/\Delta\mu\varepsilon)_{Ax}} = \frac{(\Delta\mu\varepsilon)_{Ax}}{(\Delta\mu\varepsilon)_{Hoop}} \tag{3}$$

There are differences between the two approaches for the Ax. 0 and Hoop 1 data, but the Ax. 2 and Hoop 3 data compare favorably.

Specimen 1st 1also was tested at various ring orientations, as discussed previously. Figures 13a through 13f show the axial versus hoop strains for gage pairs Ax. 0 and Hoop 1gage pairs Ax. 2 and Hoop 3 for various ring orientations. The data for ring orientation 315º are not included because the strains were small and did not lend themselves to this method of presentation. Table 10 gives the slopes of the data shown in Figure 13. As would be expected, there is a wide range of slopes because of the gage positions relative to the top of the ring. This is consistent with the data given in Table 7, the ring stiffness for various ring orientations for Specimen 1st 1. The data for these tests can also be compared using the method described above (i.e., Eqn. 3 and Table 5). These comparisons are given in Table 10. The comparisons are in reasonable agreement.

References

Young, Warren C. (1989). Roark's Formulas for Stress & Strain, Sixth Edition, McGraw-Hill Book Co., 763 p.

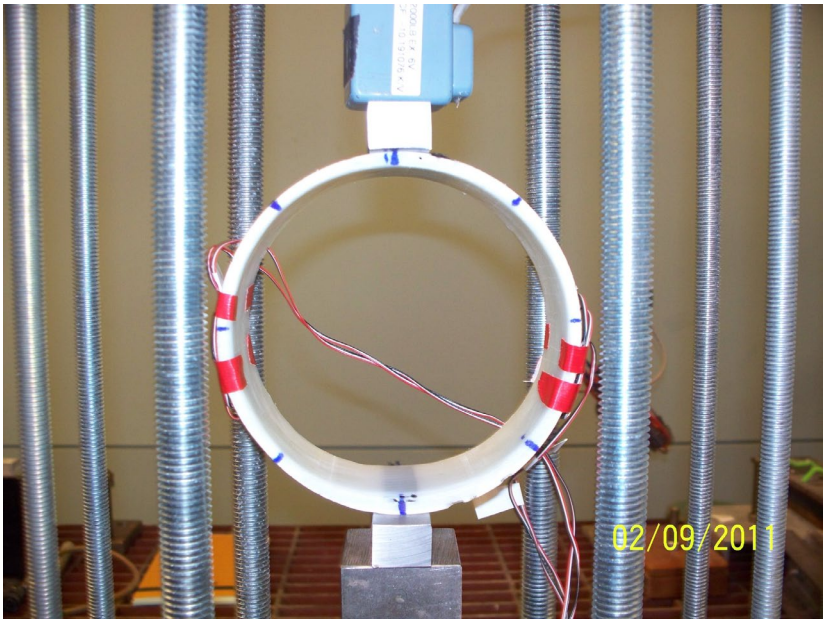

Photo 1. Experimental Setup for Ring Compression Testing, Specimen 1st 1 with Gages at Springlines (90º and 270 º)

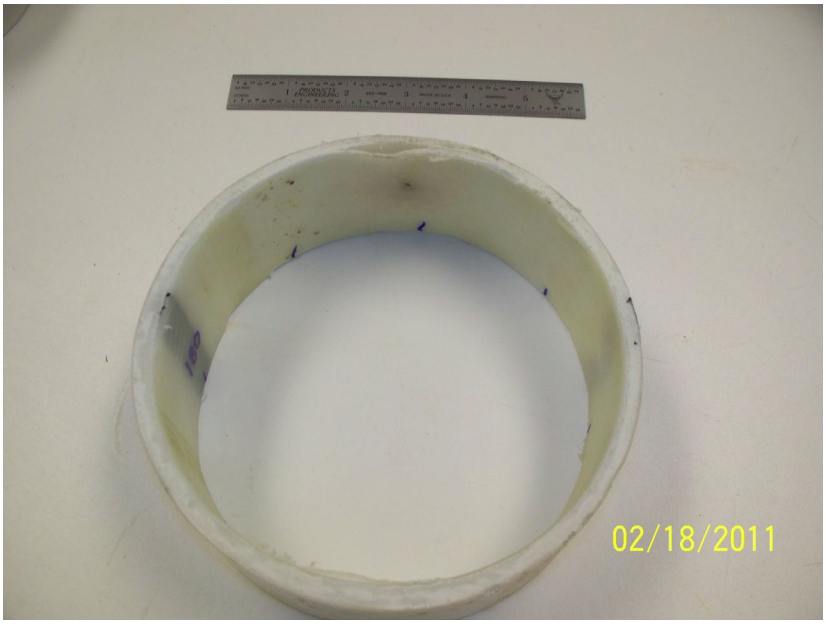

Photo 2. Delamination of Specimen 3S at 270º Springline.

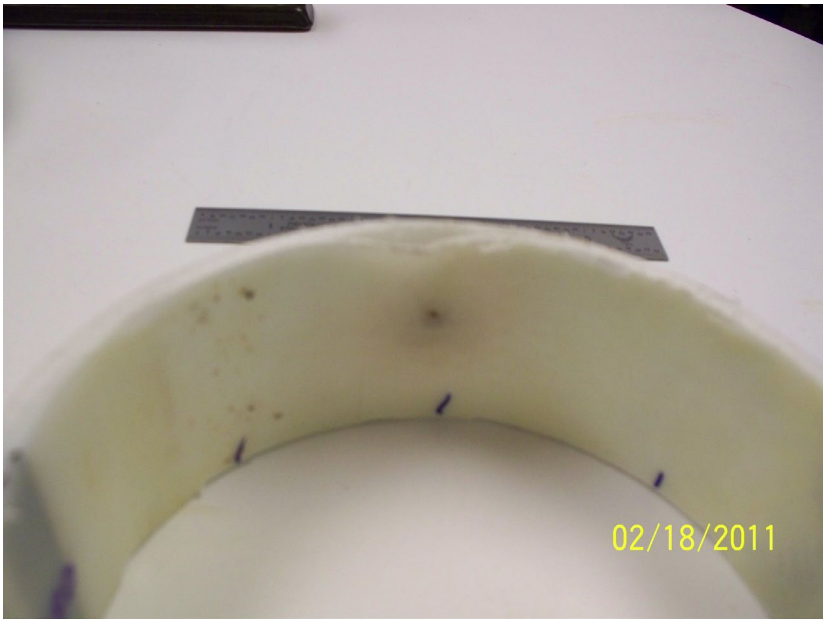

Photo 3. Interior Defect in Specimen 3S at 270º Springline

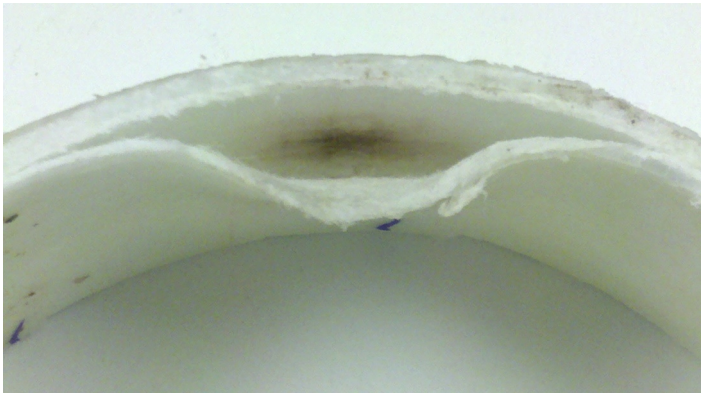

Photo 4. Interliner Defect in Specimen 3S at 270º Springline

Photo 5. Ring 1S Prior to Test to Failure

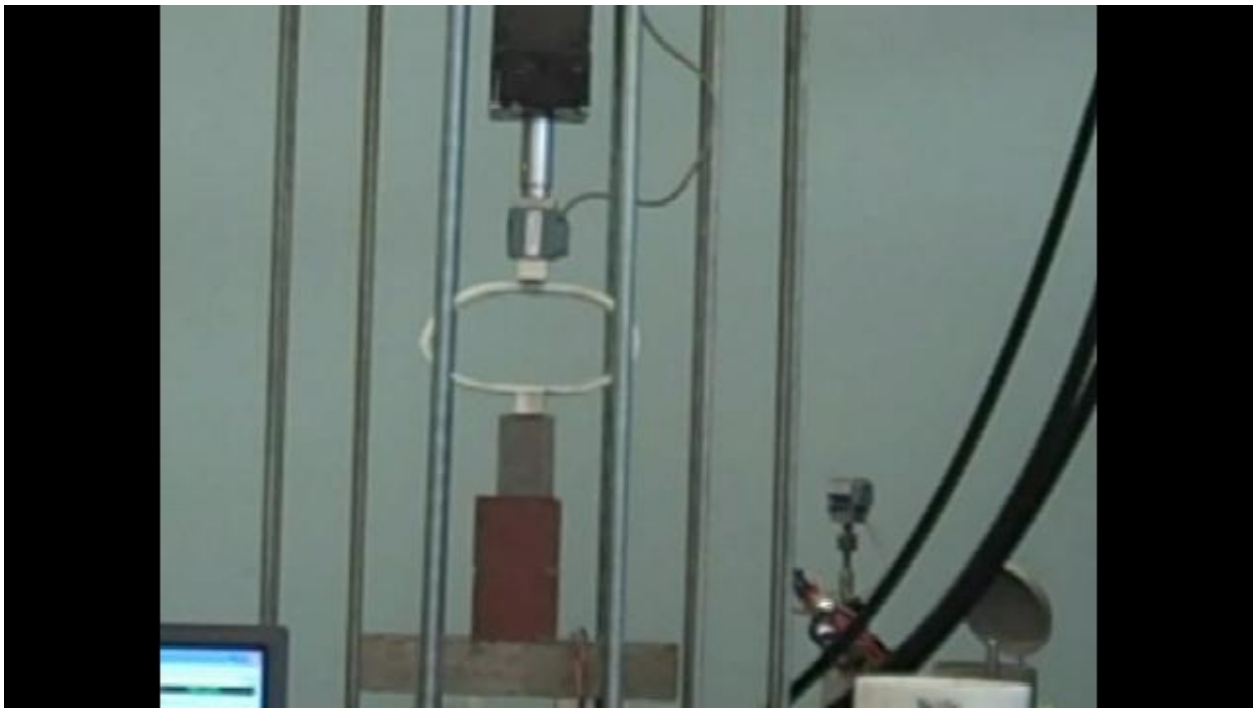

Photo 6. Ring 1S Highly Deformed

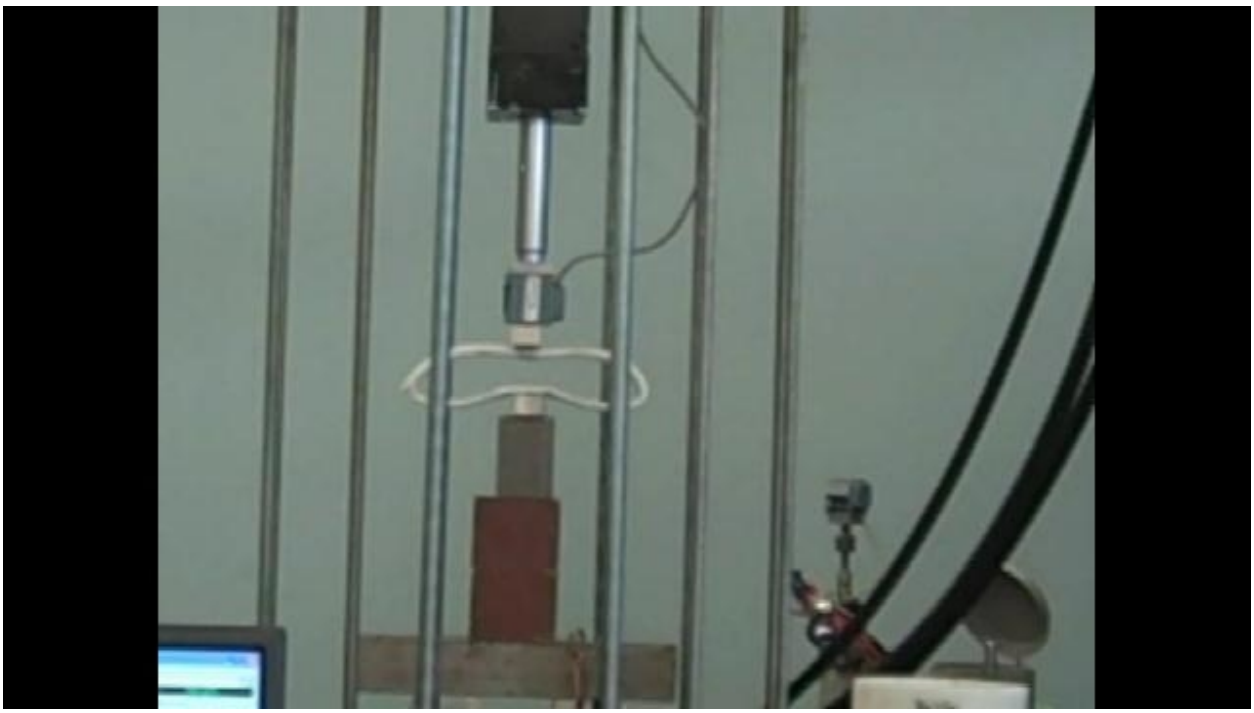

Photo 7. Ring 1S at Extreme Deformation

Table 1. Ring Compression Test Descriptions

Specimen	Test Date	Description
1st 1	Feb 01, 2011	Strain gages placed on the outside springlines to measure hoop and axial strains. Four load cycles. 1 @ 0 – 15 lb, 2 @ 0 – 20 lb, 1 @ 0 – 30 lb.
	Feb. 08, 2010	Specimen tested at various orientations. 0, 90, 135, 180, 225, 315, and 360º.
	Feb. 16, 2010	Test to failure.
1st 1		
1st 2	Feb. 10, 2011	Nine load cycles. 2 @ 0 – 35 lb, 2 @ 0 – 50 lb, 2 @ 0 – 65 lb, 2 @ 0 – 80 lb, 1 @ 0 – 100 lb.
1N	Feb. 10, 2011	Eight load cycles. 2 @ 0 – 35 lb, 2 @ 0 – 55 lb, 2 @ 0 – 85 lb, 2 @ 0 – 100 lb.
	Feb. 16, 2010	Test to failure.
1S	Feb. 10, 2011	Eight load cycles. 2 @ 0 – 35 lb, 2 @ 0 – 55 lb, 2 @ 0 – 85 lb, 2 @ 0 – 110 lb.
	Feb 16, 2011	Test to Failure.
2N	Feb. 10, 2011	Eight load cycles. 2 @ 0 – 35 lb, 2 @ 0 – 55 lb, 2 @ 0 – 85 lb, 2 @ 0 – 110 lb.
2S	Feb. 10, 2011	Eight load cycles. 2 @ 0 – 35 lb, 2 @ 0 – 55 lb, 2 @ 0 – 85 lb, 2 @ 0 – 110 lb.
3N	Feb. 10, 2011	Seven load cycles. 2 @ 0 – 35 lb, 2 @ 0 – 55 lb, 1 @ 0 – 85 lb, 2 @ 0 – 110 lb.
3S	Feb. 10, 2011	Three load cycles. 2 @ 0 – 35 lb, 1 @ 0 – 50 lb.

Table 2. Force-Strain Data from Specimen 1st 1

	$\Delta F / \Delta \mu\varepsilon$ (lb /με)			
Cycle	Ax. 0	Hoop 1	Ax. 2	Hoop 3
1	-0.114427 $r^2 = 0.998$	0.021481 $r^2 = 0.999$	-0.162914 $r^2 = 0.998$	0.016301 $r^2 = 0.999$
2	-0.116491 $r^2 = 0.999$	0.021485 $r^2 = 0.999$	-0.160501 $r^2 = 0.996$	0.016329 $r^2 = 0.999$
3	-0.117249 $r^2 = 0.999$	0.0216478 $r^2 = 0.999$	-0.163968 $r^2 = 0.999$	0.016369 $r^2 = 0.999$
4	-0.116575 $r^2 = 0.999$	0.021396 $r^2 = 0.999$	-0.158821 $r^2 = 0.996$	0.016322 $r^2 = 0.999$
Average	-0.116186	0.021503	-0.161551	0.016330
Std. Dev	0.00122	0.000105	0.002328	0.000028
COV (%)	-1.05%	0.49%	-1.44%	0.17%

Table 3. Ring Stiffnesses for Specimen 1st 1 at Various Angles.

	Circumferential Angle at Top of Ring						
Ring Stiffness,	0º	45º	135º	180º	225º	315º	360º
$\Delta F / \Delta \delta_V$ (lb/in.)	226	178	171	219	172	163	216

Table 4. Position of Gage Pairs Relative to Top of Loaded Ring.

	Gage Pair and Relative Location	
	Ax. 0 and Hoop 1	Ax. 2 and Hoop 3
Ring Orientation (degrees)	Circumferential Angle of Gage Pair Relative to Top of Ring (degrees)	
0	90	270
45	45	225
90		
135	315	135
180	270	90
225	225	45
270		
315	135	315
360	90	270

Table 5. Force-Strain Data from Specimen 1st 1, Second Testing Event

	ΔF / Δμε (lb /με)			
Orientation	Ax. 0	Hoop 1	Ax. 2	Hoop 3
0º	-0.119063 $r^2 = 0.999$	0.021195 $r^2 = 0.999$	-0.167088 $r^2 = 0.997$	0.016379 $r^2 = 0.999$
180º	-0.114545 $r^2 = 0.999$	0.020464 $r^2 = 0.999$	-0.157690 $r^2 = 0.990$	0.016715 $r^2 = 0.999$
Average	-0.116804	0.020829	-0.162389	0.016547

Table 6. Ring Geometry Measurements

Ring								
	1st 1		1st 2		1N		1S	
Degrees	t_w (in.)	D (in.)	t_w (in.)	D (in.)	t_w (in.)	D (in.)	t_w (in.)	D (in.)
0	0.240	6.017	0.239	6.007	0.244	6.012	0.260	5.998
45	0.245	5.972	0.214	6.021	0.234	6.016	0.254	6.042
90	0.221	6.004	0.262	6.034	0.248	5.990	0.218	6.002
135	0.265	6.015	0.210	5.954	0.238	5.965	0.236	5.985
180	0.390		0.364		0.332		0.349	
225	0.220		0.270		0.280		0.294	
270	0.254		0.210		0.284		0.285	
315	0.238		0.229		0.245		0.280	
Avg. (in.)	0.259	6.002	0.250	6.004	0.263	5.996	0.272	6.007
Stdev (in.)	0.055	0.021	0.024	0.035	0.006	0.023	0.019	0.025
Min (in.)	0.220	5.972	0.210	5.954	0.234	5.965	0.218	5.985
Max (in.)	0.390	6.017	0.364	6.034	0.332	6.016	0.349	6.042

Ring								
	2N		2S		3N		3S	
Degrees	t_w (in.)	D (in.)	t_w (in.)	D (in.)	t_w (in.)	D (in.)	t_w (in.)	D (in.)
0	0.261	5.971	0.270	6.018	0.266	5.992	0.266	5.957
45	0.248	6.002	0.249	6.012	0.288	5.997	0.242	6.000
90	0.249	5.994	0.224	5.999	0.272	5.981	0.290	6.058
135	0.240	6.007	0.230	5.976	0.254	5.972	0.288	6.024
180	0.344		0.305		0.318		0.356	
225	0.302		0.249		0.256		0.269	
270	0.256		0.270		0.261		0.268	
315	0.252		0.264		0.268		0.274	
Avg. (in.)	0.269	5.994	0.258	6.001	0.273	5.986	0.282	6.010
Stdev (in.)	0.009	0.016	0.021	0.019	0.014	0.011	0.022	0.042
Min (in.)	0.240	5.971	0.224	5.976	0.254	5.972	0.242	5.957
Max (in.)	0.344	6.007	0.305	6.018	0.318	5.997	0.356	6.058

Table 7. Ring Stiffnesses for All Tests.

	Specimen							
	1st 1	1st 2	1N	1S	2N	2S	3N	3S
Orientation	$\Delta F / \Delta \delta_v$ (lb/in.)							
0º	232	172	220	237	233	232	271	195
0º	226							
45 º	178							
135º	171							
180º	219							
225º	172							
316º	163							
360º	216							

Table 8. Flexural Young's Modulus, E, for All Tests.

	Specimen							
	1st 1	1st 2	1N	1S	2N	2S	3N	3S
Orientation	E, ksi							
0º	594	441	564	607	597	594	694	500
0º	579							
45 º	456							
135º	438							
180º	561							
225º	441							
316º	418							
360º	553							

Table 9. Slopes of Gage Pair Strains, Specimen 1st 1

	Slopes of Gage Pair Strains from Figure 12		$\frac{(\Delta\mu\varepsilon)_{Ax}}{(\Delta\mu\varepsilon)_{Hoop}}$ from Eqn. 3 and Table 2 Slopes	
Cycle	Ax. 0 / Hoop 1	Ax. 2 / Hoop 3	Ax. 0 / Hoop 1	Ax. 2 / Hoop 3
1	-0.132 $r^2 = 0.999$	-0.100 $r^2 = 0.999$	-0.188	-0.100
2	-0.183 $r^2 = 0.999$	-0.101 $r^2 = 0.997$	-0.116	-0.102
3	-0.132 $r^2 = 0.999$	-0.100 $r^2 = 0.999$	-0.117	-0.100
4	-0.183 $r^2 = 0.999$	-0.102 $r^2 = 0.999$	-0.117	-0.103

Table 10. Slopes of Gage Pair Strains for Various Ring Orientations, Specimen 1st 1

	Slopes of Gage Pair Strains from Figure 13		$\frac{(\Delta\mu\varepsilon)_{Ax}}{(\Delta\mu\varepsilon)_{Hoop}}$ from Eqn. 3 and Table 5 Slopes	
Ring Orientation	Ax. 0 / Hoop 1	Ax. 2 / Hoop 3	Ax. 0 / Hoop 1	Ax. 2 / Hoop 3
0º	-0.127 $r^2 = 0.999$	-0.098 $r^2 = 0.999$	-0.178	-0.098
45º	-0.178 $r^2 = 0.999$	-0.0.098 $r^2 = 0.999$		
135º	-0.459 $r^2 = 0.994$	-0.217 $r^2 = 0.993$		
180º	-0.179 $r^2 = 0.999$	-0.106 $r^2 = 0.999$	-0.179	-0.106
225º	-0.300 $r^2 = 0.999$	-0.130 $r^2 = 0.996$		
315º	-	-		
360º	-0.174 $r^2 = 0.999$	-0.094 $r^2 = 0.986$		

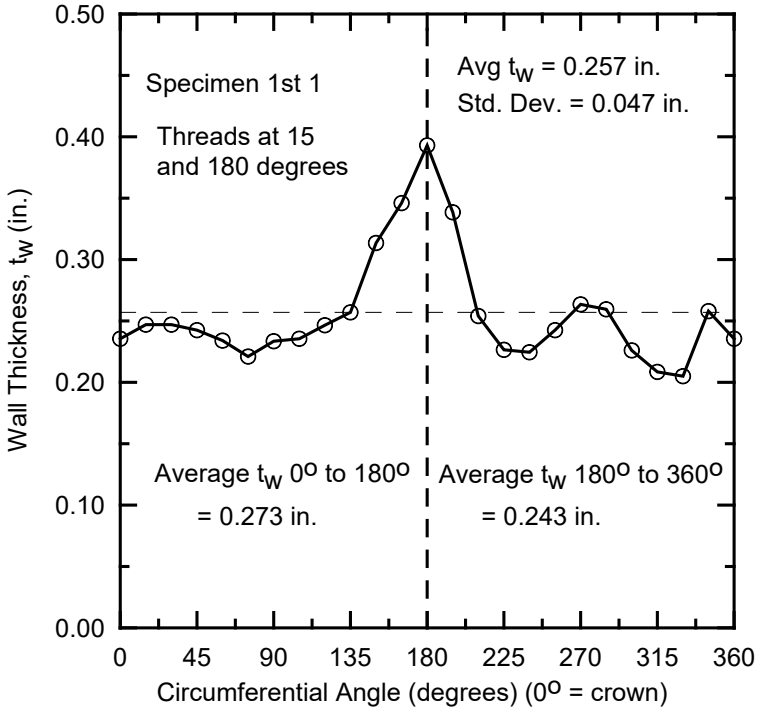

Figure 1. Liner Wall Thicknesses for Ring Test Specimen 1st 1

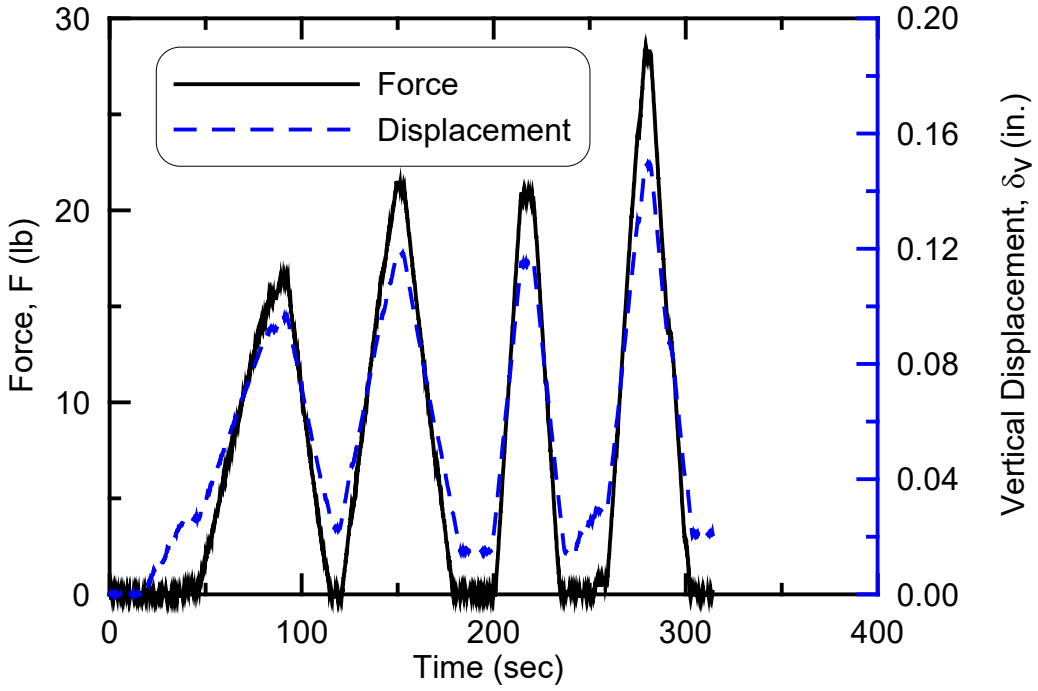

Figure 2. Force and Displacement versus Time for Specimen 1st 1

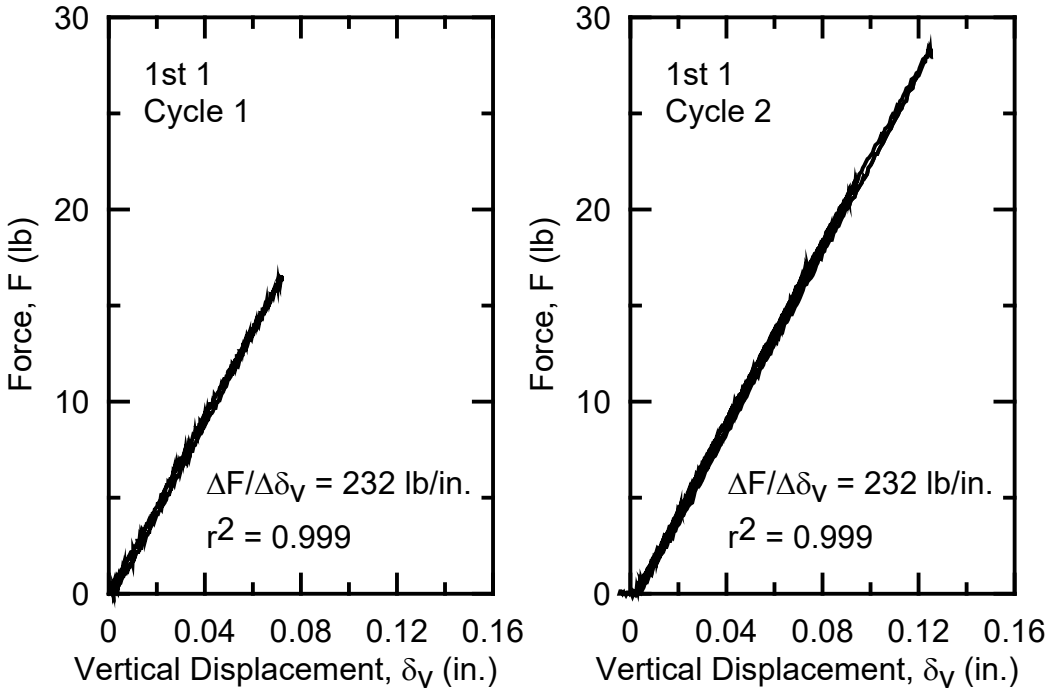

a) Cycle 1

b) Cycle 2

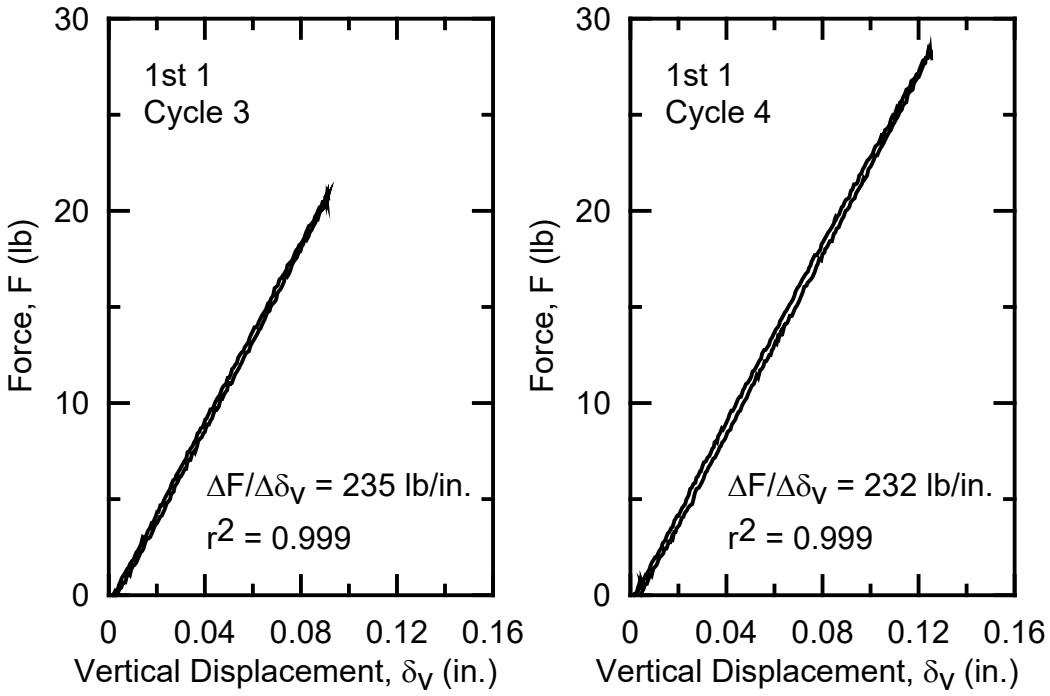

c) Cycle 3

d) Cycle 4

Figure 3. Force-Displacement for Specimen 1st 1

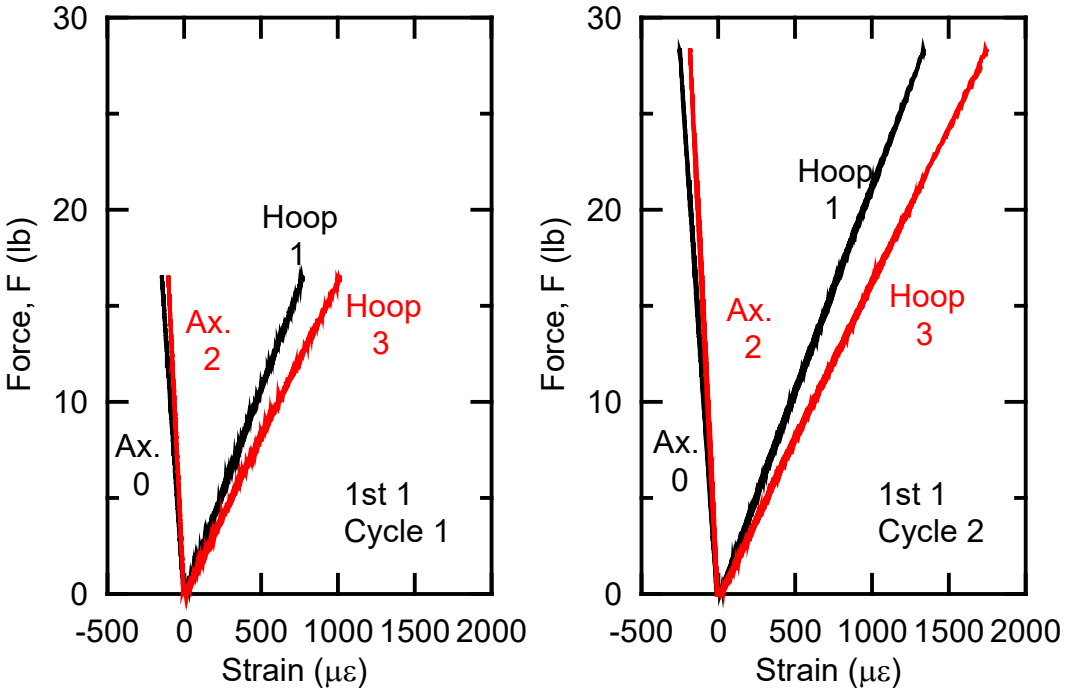

a) Cycle 1

b) Cycle 2

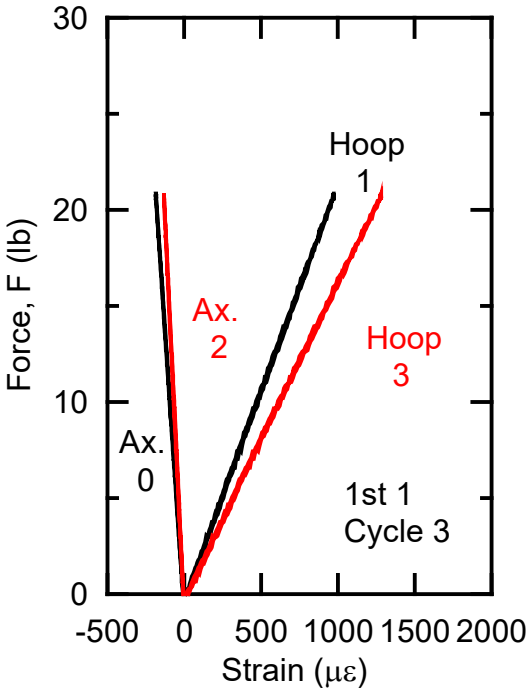

c) Cycle 3

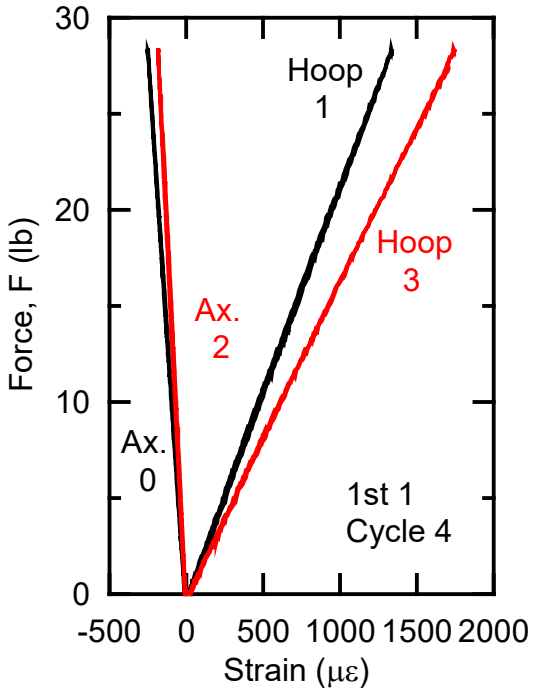

d) Cycle 4

Figure 4. Force-Strain for Specimen 1st 1

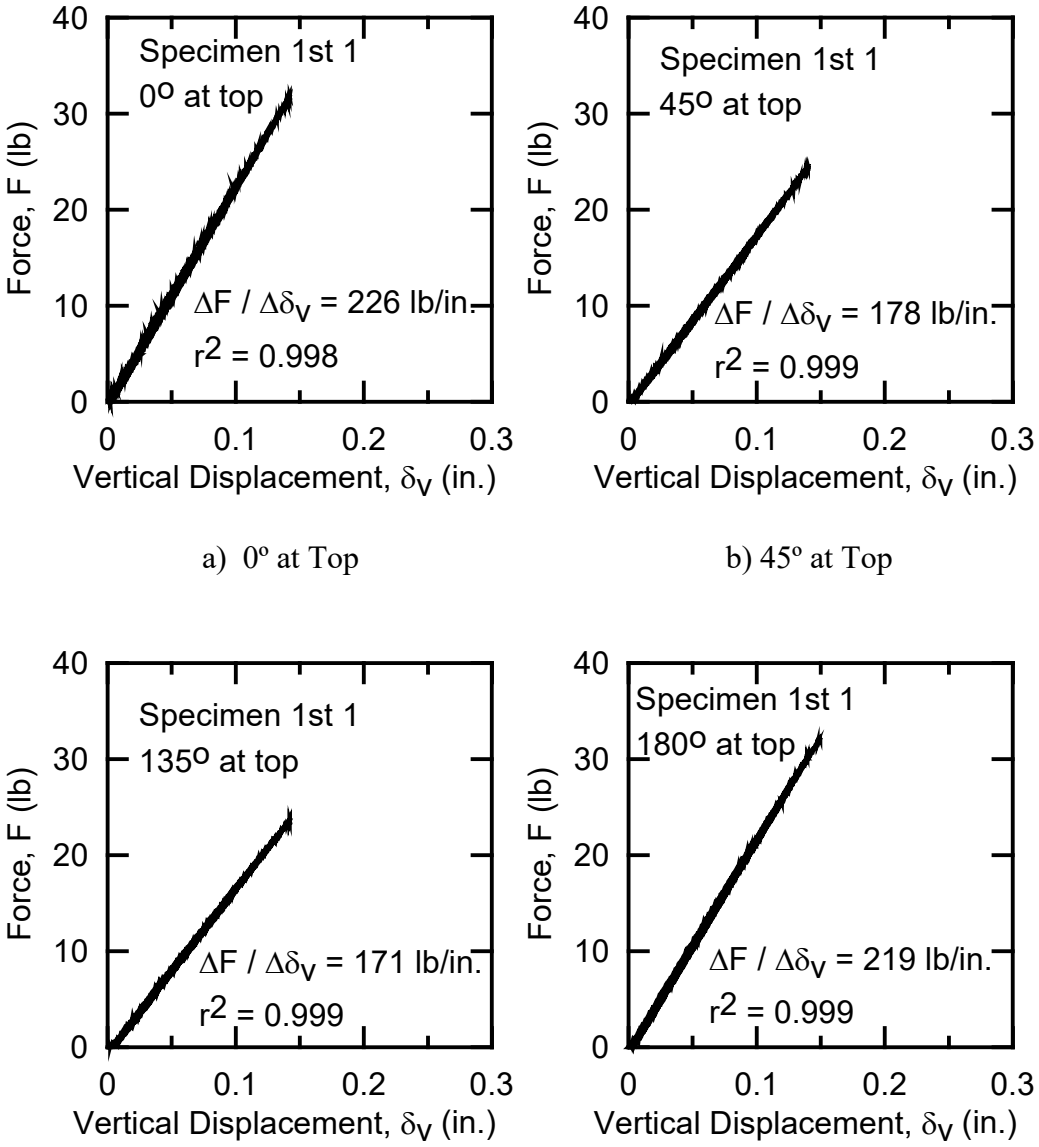

a) 0º at Top

b) 45º at Top

c) 135º at Top

d) 180º at Top

Figure 5. Force – Vertical Displacement for Various Ring Orientations

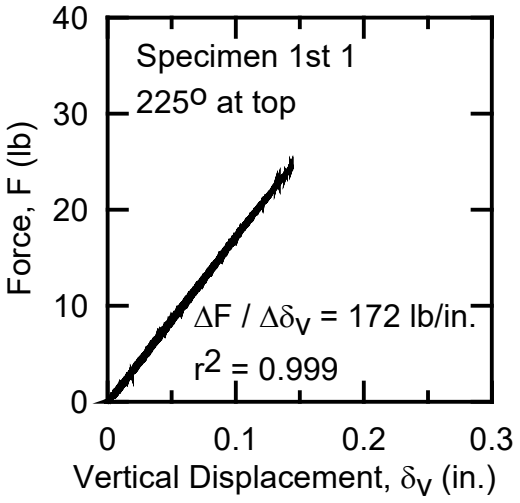

e) 225º at Top

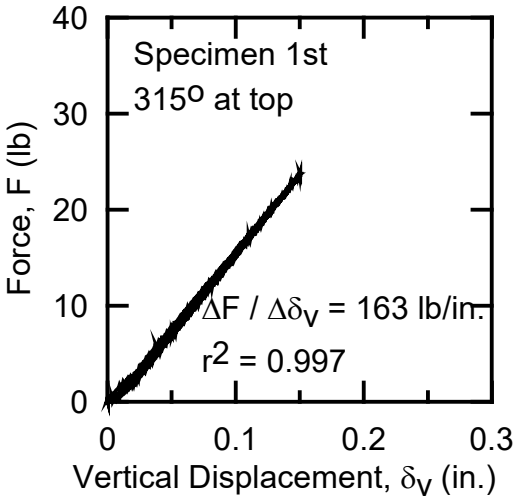

f) 315º at Top

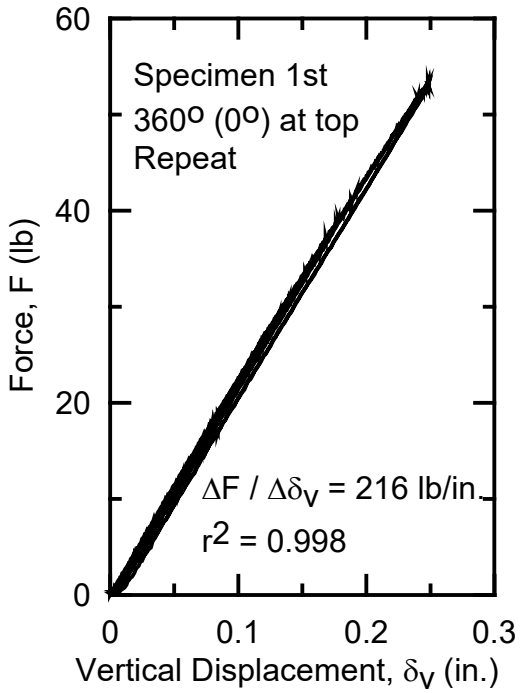

g) 360º at Top

Figure 5. Force – Vertical Displacement for Various Ring Orientations (completed)

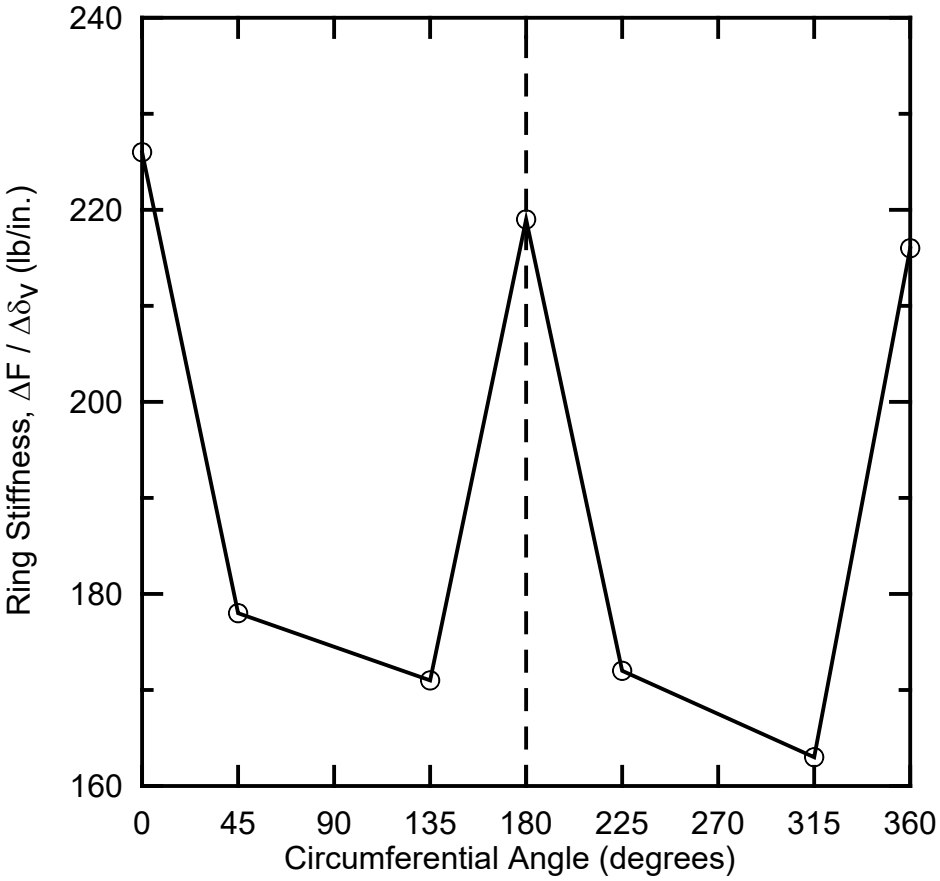

Figure 6. Ring Stiffness versus Circumferential Angle

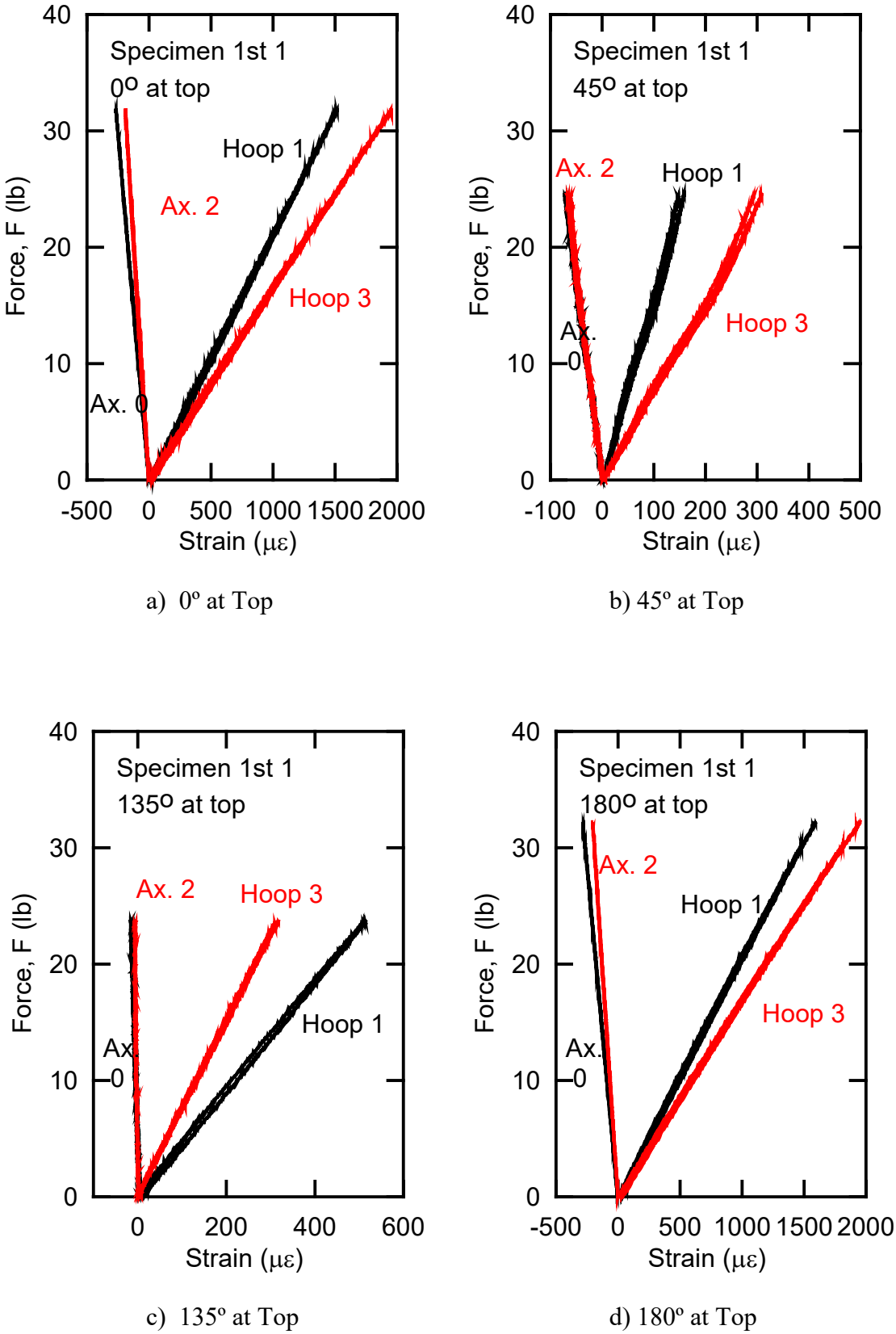

a) 0º at Top

b) 45º at Top

c) 135º at Top

d) 180º at Top

Figure 7. Force – Strain Various Ring Orientations

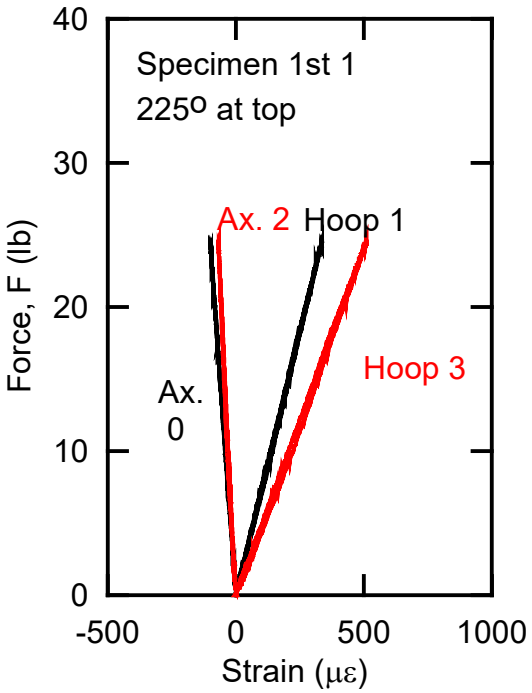

e) 135º at Top

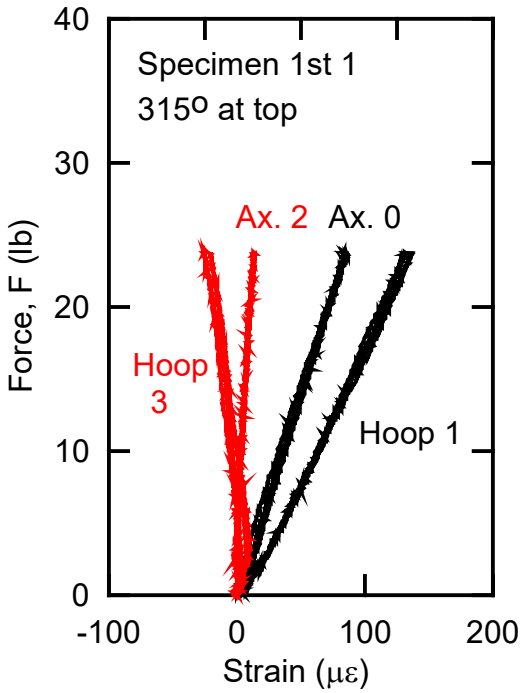

f) 315º at Top

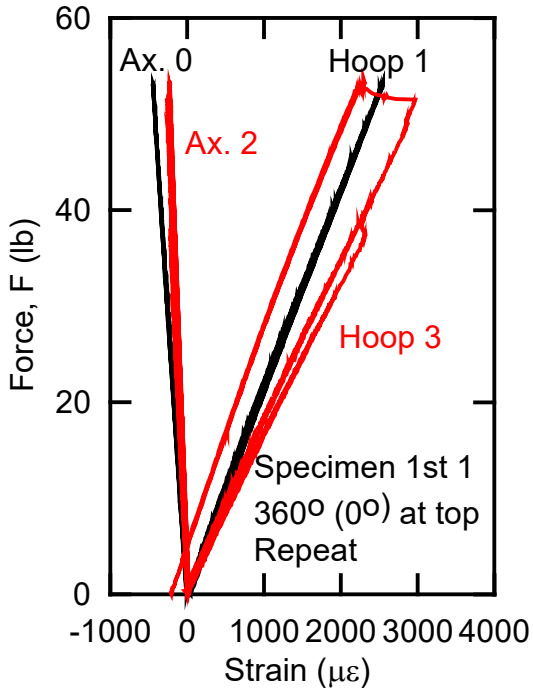

g) 360º at Top

Figure 7. Force – Strain Various Ring Orientations (completed)

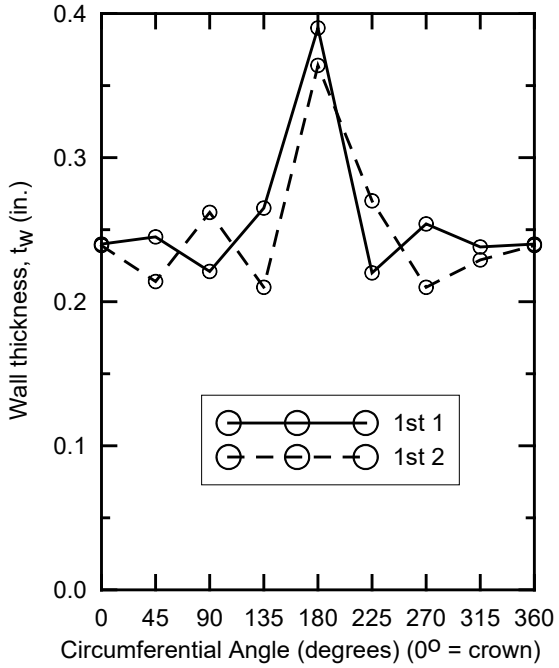

a) Wall Thickness for 1st 1 and 1st 2

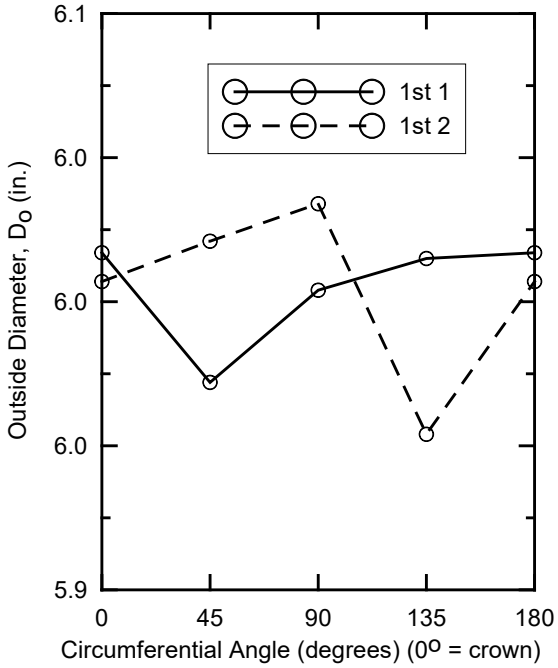

b) Diameters for 1st 1 and 1st 2

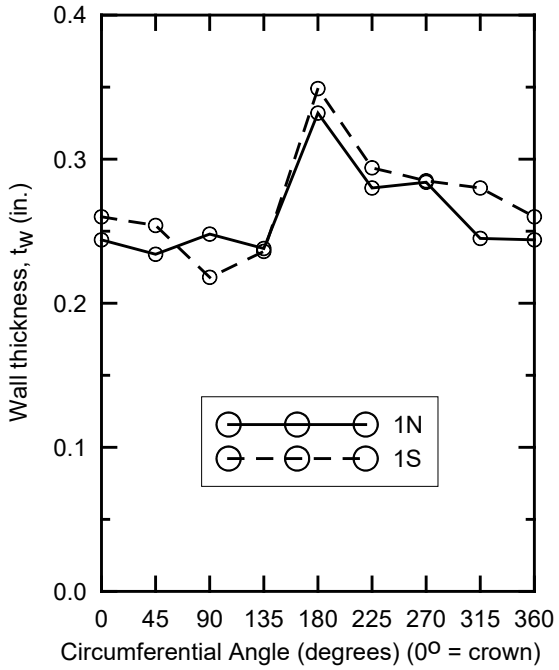

c) Wall Thickness for 1st 1N and 1S

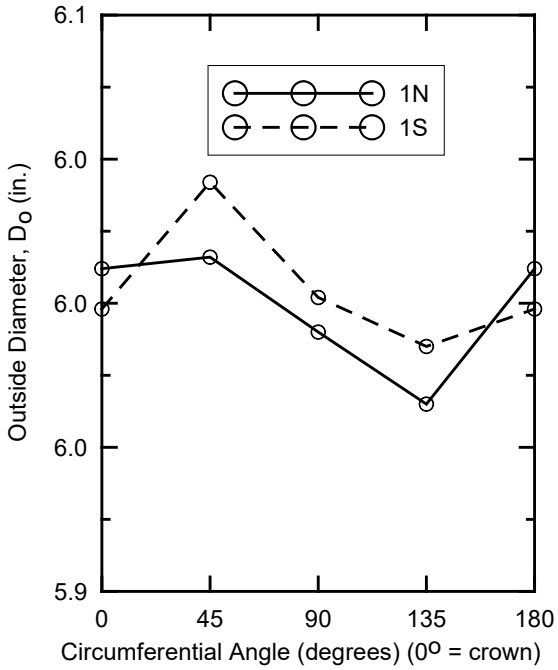

d) Diameters for 1N and 1S

Figure 8. Wall Thicknesses and Diameters for Ring Compression Tests

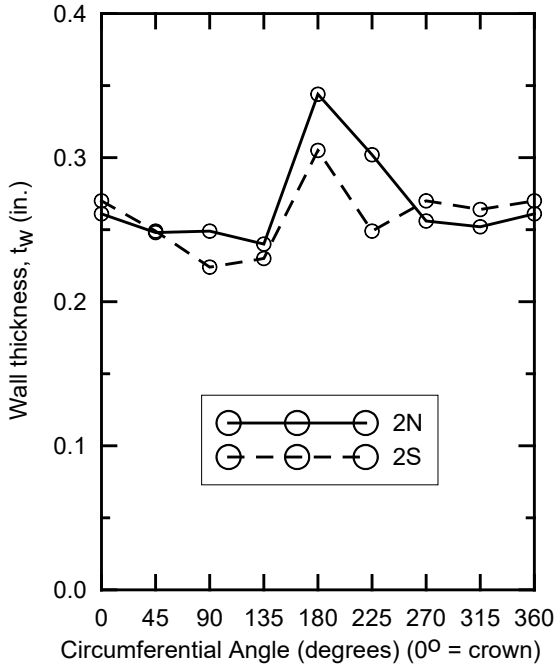

e) Wall Thickness for 1st 2N and 2S

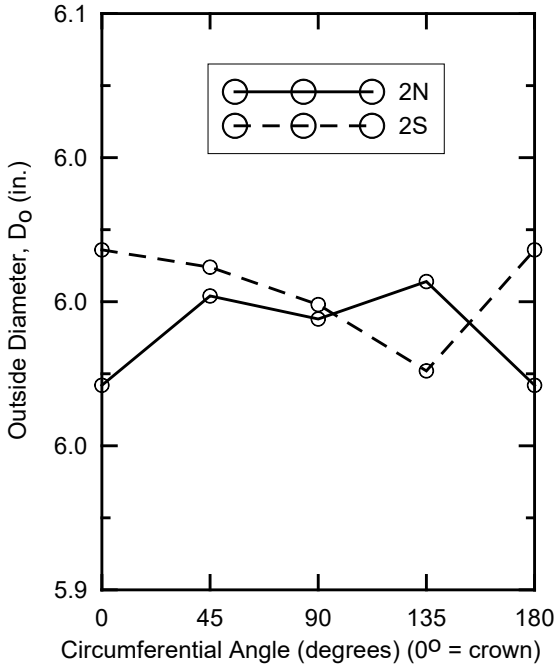

f) Diameters for 2N and 2S

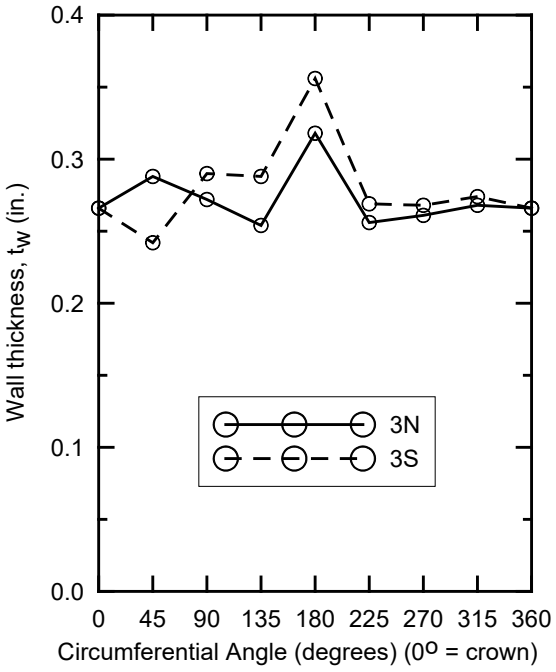

g) Wall Thickness for 1st 3N and 3S

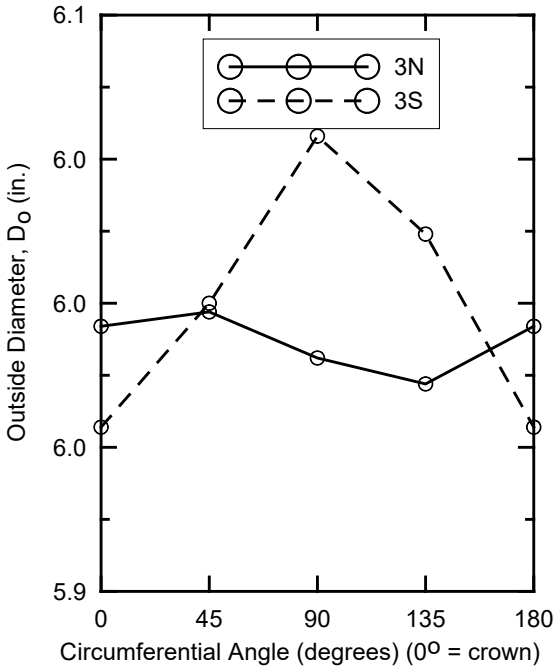

h) Diameters for 3N and 3S

Figure 8. Wall Thicknesses and Diameters for Ring Compression Tests (completed)

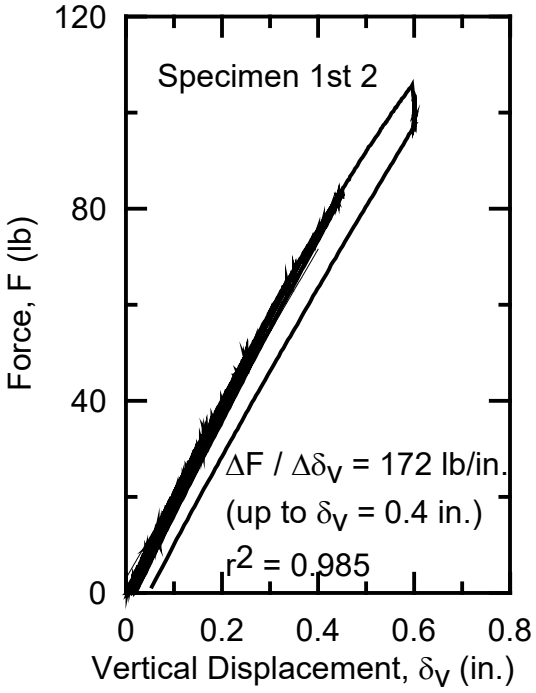

a) Specimen 1st 2

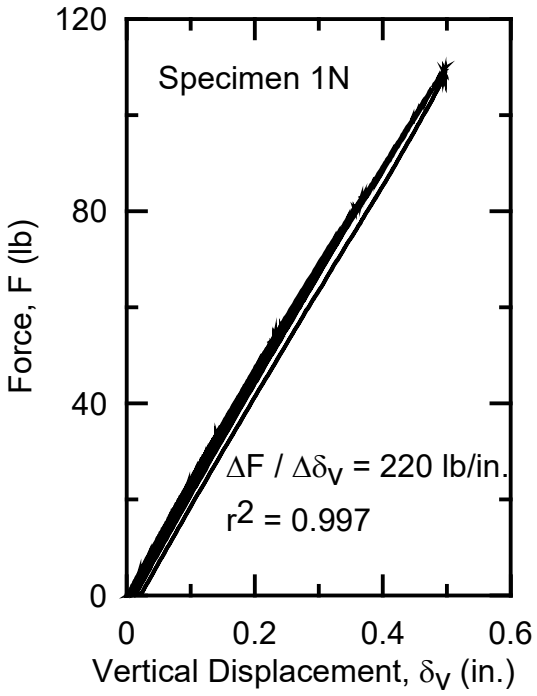

b) Specimen 1N

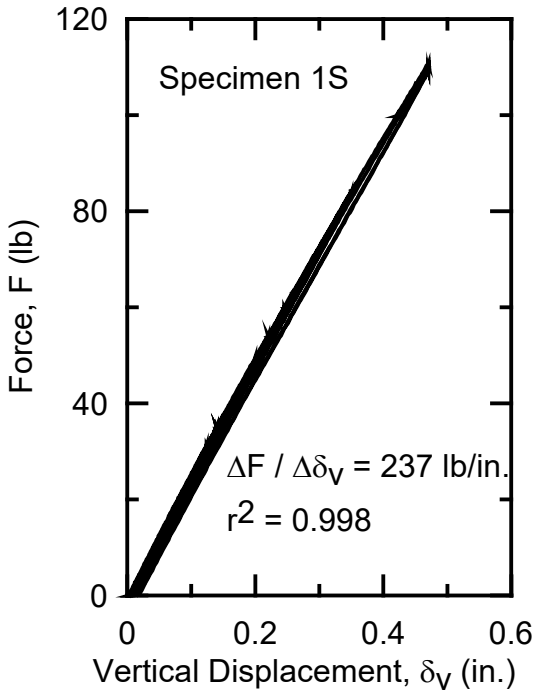

c) Specimen 1S

Figure 9. Force – Vertical Displacement for Remaining Ring Compression Tests

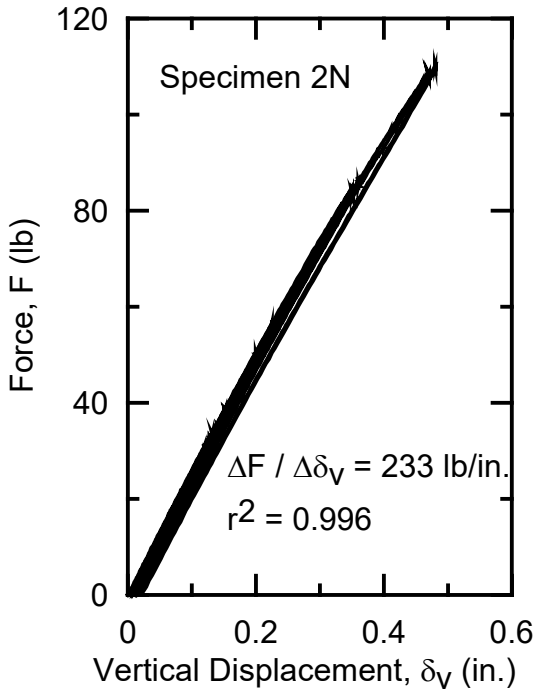

d) Specimen 2N

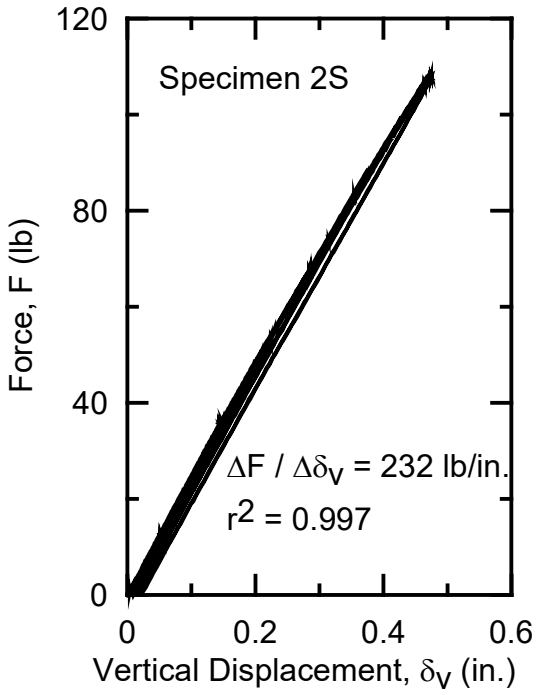

e) Specimen 2S

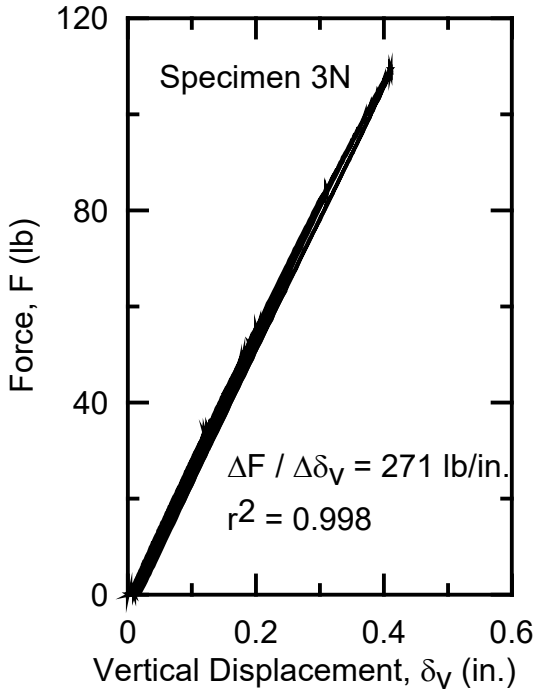

f) Specimen 3N

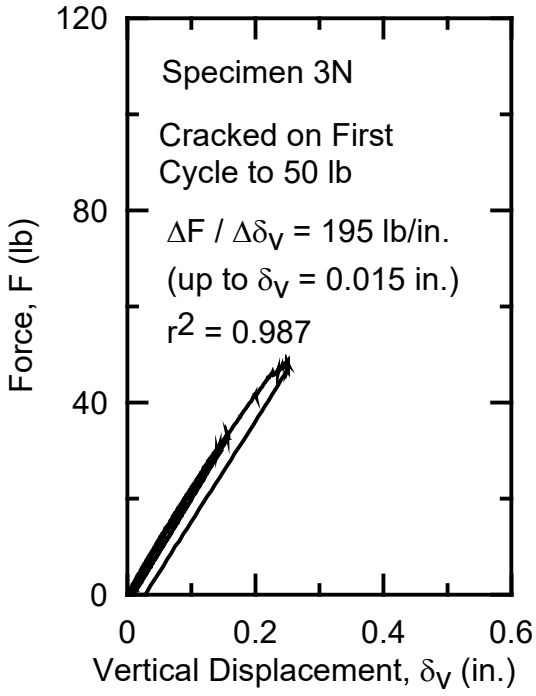

g) Specimen 3S

Figure 9. Force – Vertical Displacement for Remaining Ring Compression Tests (completed)

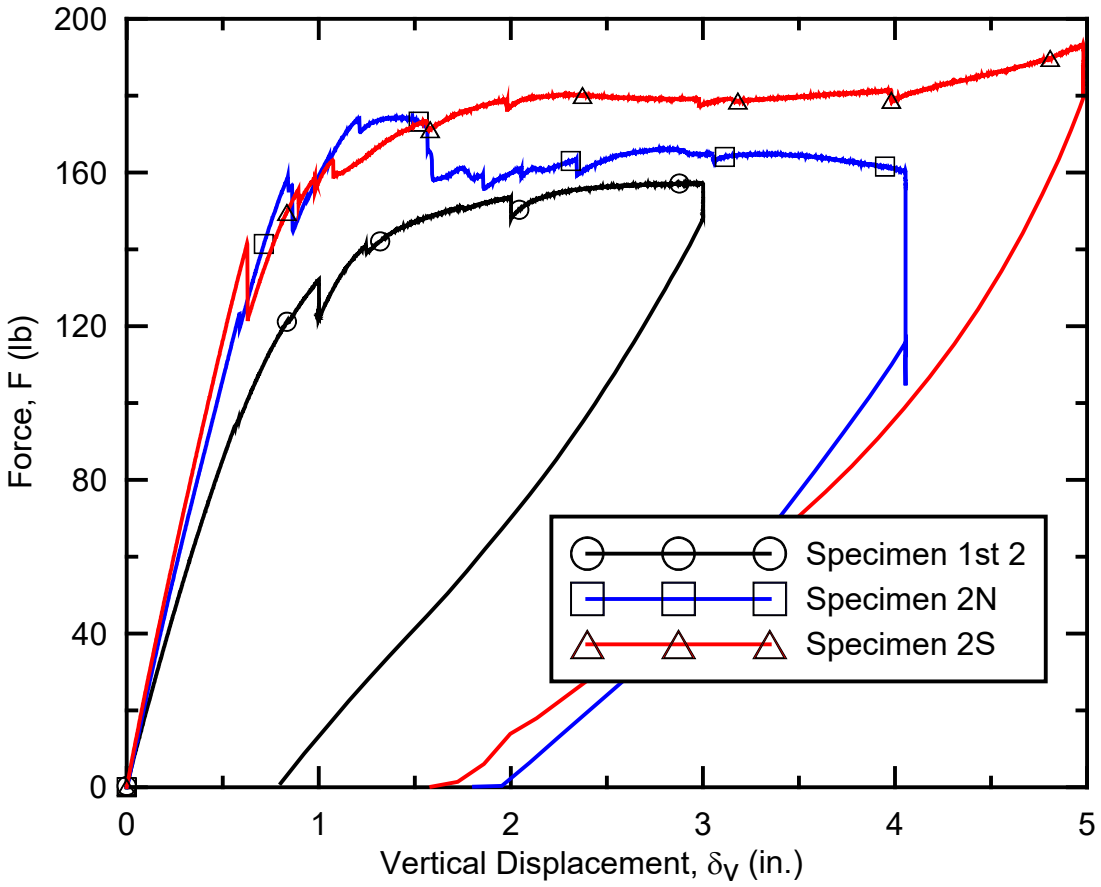

Figure 10. Ring Tests to Failure

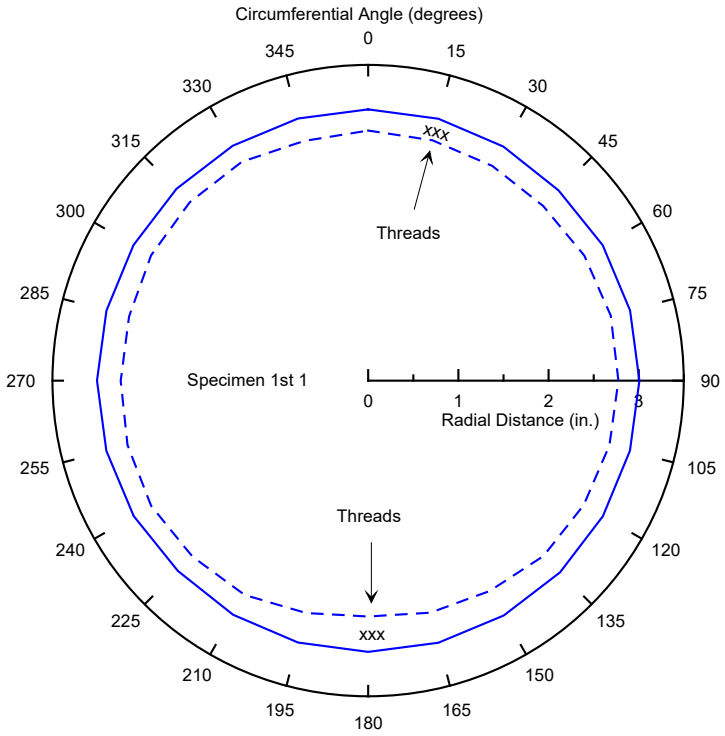

a) Specimen 1st 1

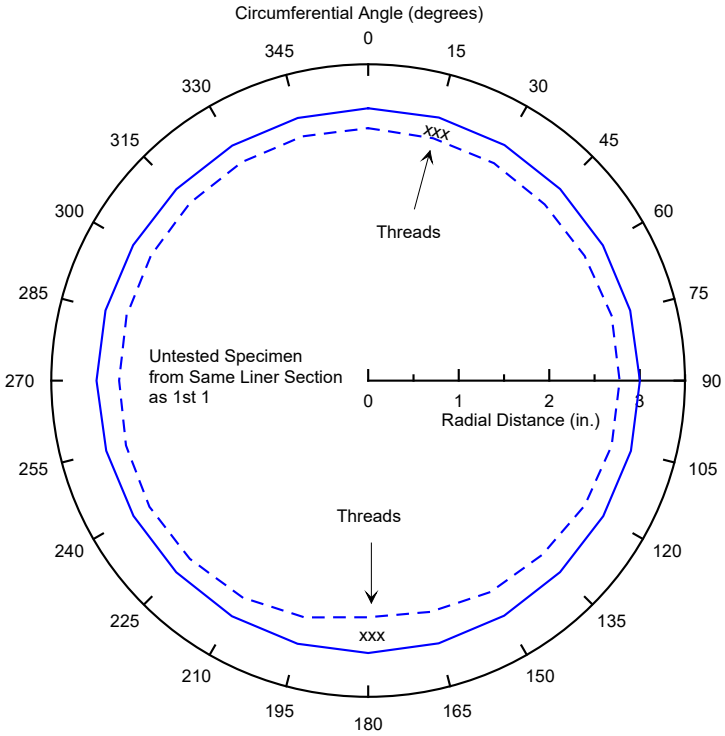

b) Untested Specimen

Figure 11. Ring Cross Section Geometries

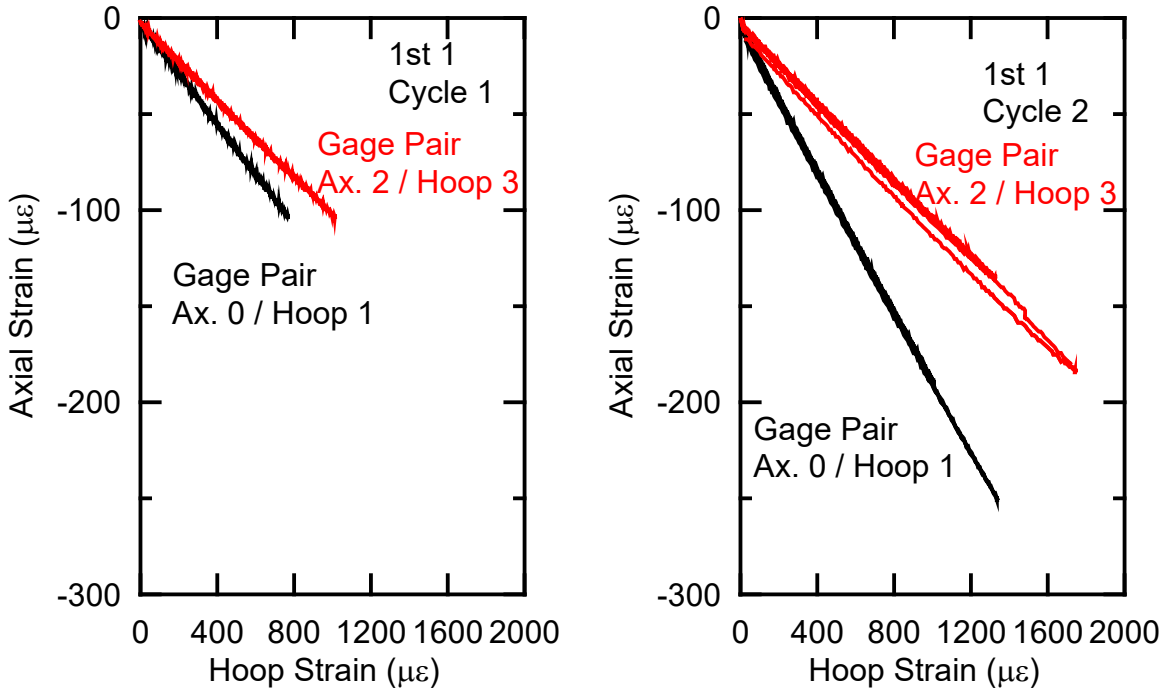

a) Cycle 1

b) Cycle 2

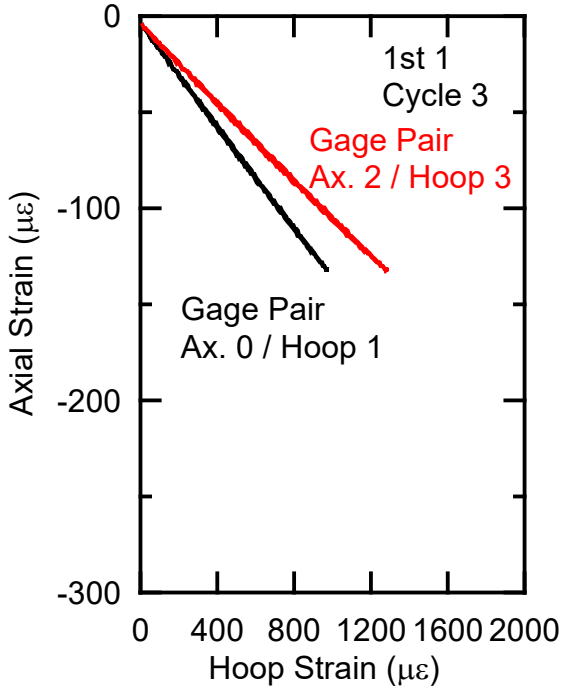

c) Cycle 1

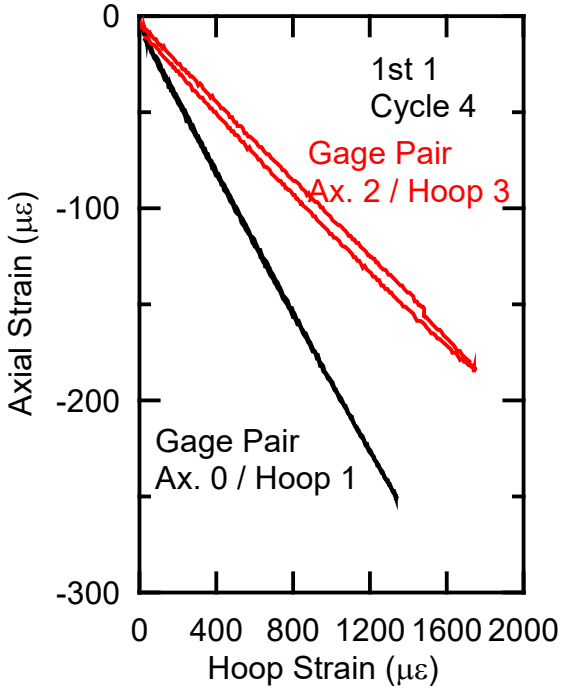

d) Cycle 2

Figure 12. Gage Pair Strains, Specimen 1st 1

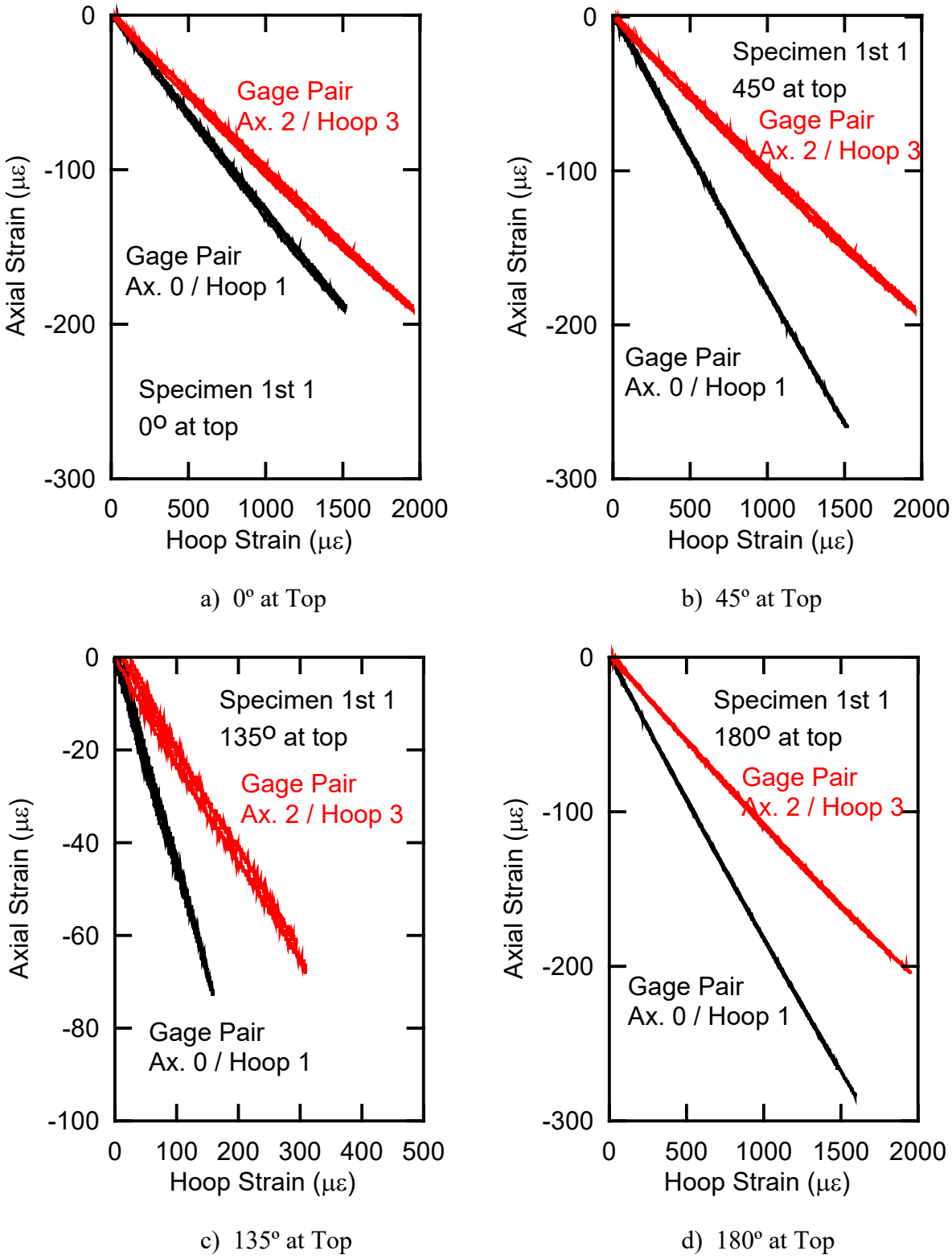

a) 0º at Top

b) 45º at Top

c) 135º at Top

d) 180º at Top

Figure 13. Gage Pair Strains for Various Ring Orientations

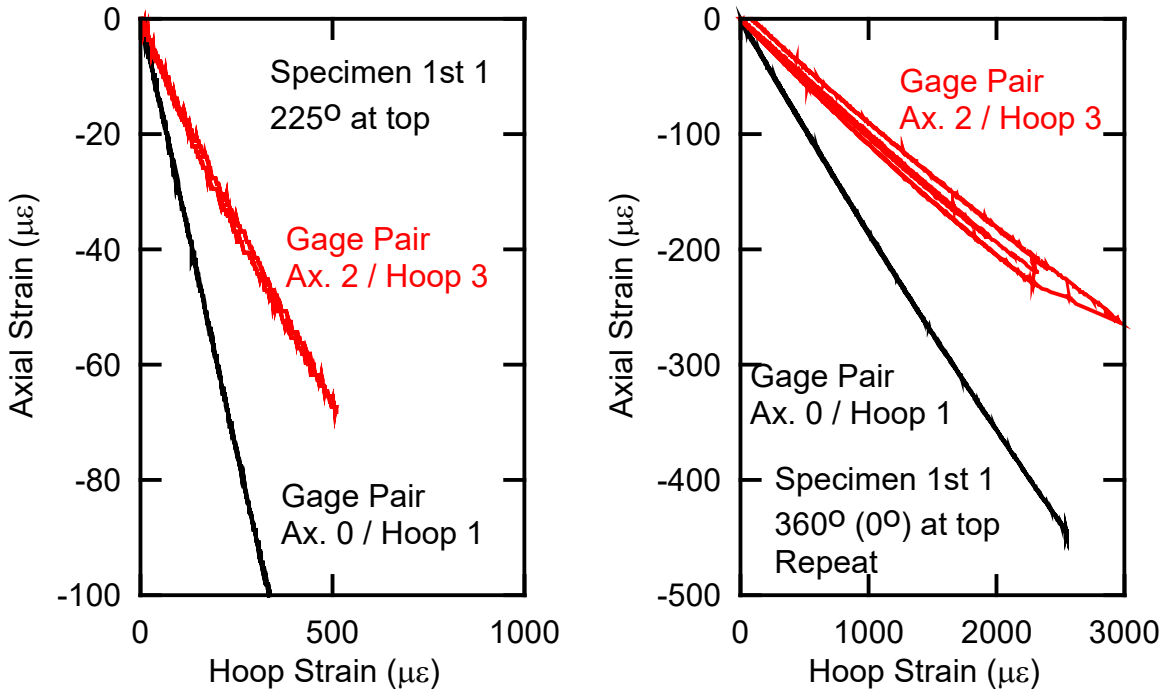

e) 135º at Top

f) 180º at Top

Figure 13. Gage Pair Strains for Various Ring Orientations (completed)